Drying Liquid Coatings with an Evaporation Mask: Theory and Experiments

Apolline Faidherbe, Maxence Wilmet, Jérémie Teisseire, François Lequeux, Laurence Talini

Drying liquid coatings with an evaporation mask: theory and experiments

Apolline Faidherbe,[†] Maxence Wilmet,[‡] Jérémie Teisseire,[‡] François Lequeux,[¶] and Laurence Talini[*,†]

[†]*CNRS, Surface du Verre et Interfaces, Saint-Gobain, 93300 Aubervilliers, France.*

[‡]*Saint-Gobain Resarch Paris, 93300 Aubervilliers, France.*

[¶]*CNRS Sciences et Ingénierie de la Matière Molle, ESPCI Paris, PSL Research University, Sorbonne Université 75005 Paris, France.*

E-mail: laurence.talini@cnrs.fr

Abstract

We report a study of the spatially varying thickness of dried films of polymer solutions resulting from a nonuniform evaporation flux. The controlled heterogeneity of the evaporation flux is imposed by placing a solid mask above the evaporating film spread on a solid substrate. At the end of drying, a depression has formed under the mask, together with overthicknesses extending from the edge of the mask and over distances that may be larger than its size. By considering the flows induced in a vertically homogeneous film, we obtain analytical solutions for the thickness profiles during drying using a linear approximation in the limits of either gravity or capillarity-driven flows.We demonstrate that gravity can play a role in the deformations of the films, even if their initial thicknesses are one order of magnitude smaller than the capillary length. In addition, we examine two possible reference states for the linear approximation, i.e. far from the mask in the film of decreasing thickness and increasing

viscosity, or under the mask where no evaporation occurs. We further compare these results with experimental ones obtained by drying thin films of polymer solutions under a mask. Both the extent and amplitude of the thickness heterogeneities of the dry film are quantitatively predicted by the linear analysis for a reference state under the mask. Our results therefore provide new insight on the patterns resulting from evaporation masks and can be generalised to minimize thickness heterogeneities in any situation in which the evaporation flux is nonuniform.

Introduction

Drying a complex fluid on a solid substrate generally results in a spatially nonuniform dry deposit. This effect was explained more than twenty years ago in the case of drops of suspensions and is known as the "coffee-stain effect".[1] The accumulation of solid particles at the contact lines of sessile drops was shown to result from a nonuniform evaporation flux: because the latter diverges at the contact line, the liquid flows from the center of the drop to its edge. Therefore, solute is advected and accumulates at the contact line, which is pinned, resulting in a ring-like dry deposit when the solvent is fully evaporated. This picture is valid provided the solute diffuses slowly enough, i.e. in the limit of large Péclet numbers, $Pe = t_{diff}/t_{ad}$ where t_{diff} and t_{ad} are characteristic times of respectively the horizontal diffusion and advection processes. This condition can be met with solid particles as solute but also with polymer coils.[2] As was shown later, divergence of the evaporation flux is not required for accumulation at the contact line,[3,4] nevertheless nonuniform evaporation fluxes are generally at the origin of heterogeneous dry deposits. The stains formed by the evaporation of sessile drops have been extensively studied in the past decades with complex fluids of diverse natures.[5,6] In particular, effects counteracting solute accumulation have been examined, and Marangoni flows resulting from concentration gradients of surfactant species have been shown to efficiently suppress coffee-stain effects.[7–9]

Similar phenomena are at stake when films of complex fluids dry on solid substrates.[10]

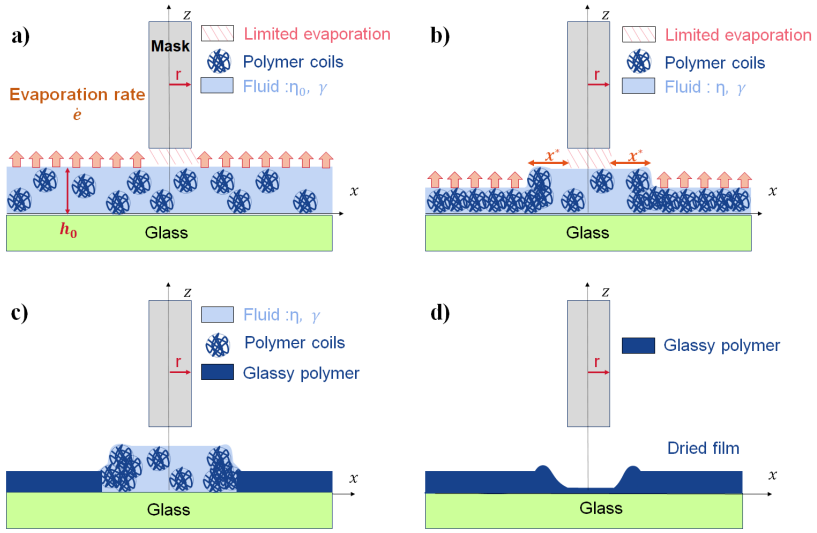

Figure 1: Schematic representation of the different steps when a thin film of complex fluid dries in presence of an evaporation mask. (a) The initially flat film is submitted to solvent evaporation at the same rate everywhere but under the mask, where it is zero. (b) The excess of liquid under the mask relaxes under the action of capillarity and gravity. (c) Solute is advected by the flow. (d) The final dry film exhibits a depression under the mask associated with a rim.

The latter situation is particularly relevant for coating applications for which control of the uniformity of the dry film is usually required. In this geometry, drying fronts have been observed to propagate either vertically, or laterally, i.e. from the edges to the centre of the film as a result of a larger evaporation flux at the edges.[11–14] Special attention has been paid to lateral fronts in films of colloidal suspensions; two fronts have been observed: a compaction front separating the suspension from a gelled phase and an additional front separating the gelled phase from the dry solid. Once drying is completed, thickness gradients extend from the edges over distances that may reach a few centimeters.[13,14] During drying, the surface of the film is deformed by the propagation of the front, and this deformation is opposed by both capillary and hydrostatic pressures. The length at which the flow caused by evaporation is balanced by the one resulting from capillarity was found to play a key role in the final morphology of the films.[14] In the case of thin liquid films, numerical resolution of the thin film equation has been performed to account for thickness heterogeneities and the results were in qualitative agreement with experiments.[13] More recently, numerical simulations reproduced

the front propagation observed in experiments[14] but failed to predict the shape of the dried film.[15]

Along a different line, Routh and Russel introduced the idea that controlled heterogeneities of the evaporation flux of a film could allow the patterning of its dried surface.[13] Actually, evaporation masks, i.e. solids placed above evaporating films and locally hindering evaporation, have been shown to effectively tune the shape of the dry deposit. A so-called evaporative lithography has been developed[16,17] ; depressions are observed just below evaporation masks, whereas solute accumulates in the region of non zero evaporation near the masks. A qualitative explanation of the pattern resulting from an evaporation mask has been given in the literature,[18] which we report here and illustrate in figure 1. As pictured in (a), what is considered is the drying of a liquid film containing a solute. The film is thin enough to remain homogeneous in the vertical direction. Solvent evaporates at a uniform rate everywhere but under an evaporation mask that hinders evaporation. More liquid therefore remains under the mask than away from it and the resulting bump further relaxes because of gravity and capillarity, while the solvent keeps evaporating, as depicted in figure 1 (b). An outward flow is generated, that carries solute away from the masked region to the nearby unmasked zone where it accumulates, as schemed in figure 1 (c). At the end of drying, a depression is hence formed below the mask, which is associated with bumps close to the edges of the mask as depicted in figure 1 (d).

A quantitative description of the thickness heterogeneities requires to model the flow and solute transport. Routh and Russel performed a numerical resolution of the lubrication equation to describe the height profile of a film resulting from an evaporation mask.[13] They assumed that the gravity related term was negligible and that the viscosity had a constant value. Other numerical resolutions or simulations have been since performed,[17] in which the influence of additional complex effects such as Marangoni flows[19] or gas blowing[20] were examined. However, in the simpler case of a single evaporation mask, the role of gravity remains elusive and the dependence of the features of the formed pattern on the different

parameters has not been quantitatively established. In the present work, we predict the extent and amplitude of thickness heterogeneities resulting from an evaporation mask with an analysis based on linearised equations. This simplification allows us to account for the increasing viscosity of the liquid film as solvent evaporates, and, in addition, to compare the effects of capillarity and gravity. We further compare our theoretical findings to experimental data obtained with polymer solutions in which Marangoni flows are negligible. We first detail the experimental systems and procedures. The theoretical analysis is further presented and, finally, predictions are compared to experimental findings in a last section.

Experimental section

In this section we describe the preparation of the polymer solutions, the experimental set-up that was used to study the effect of evaporation flux heterogeneities and measurements of the evaporation rate.

Solutions

Polystyrene solutions in toluene were prepared by adding polystyrene of molar mass $M = 1.92 \times 10^5$ g.mol^{-1} (Sigma-Aldrich) to high-purity toluene ($> 99.5\%$, VWR). The solutions were stirred at room temperature until complete dissolution before use. Solutions of volume fractions in polystyrene ϕ ranging from 0.04 to 0.25 were used. At room temperature, polystyrene solutions undergo a glass transition when the solvent content decreases. The volume fraction in polymer, ϕ_g, at which the solutions become glassy was obtained from Fox's law[21] and is $\phi_g = 0.86$.

Viscosity measurements were conducted and confirmed that the initial solutions are in the entangled semi-dilute regime. In this regime, since toluene is a good solvent for polystyrene, the viscosity increases with volume fraction according to $\eta \simeq \eta_{ref}\phi^{\nu}$ with $\nu = 3.9$[22] and $\eta_{ref} = 230$ Pa.s inferred from viscosity measurements. The latter relation does not account

for the very strong viscosity increase in the vicinity of glass transition as solvent evaporates; nonetheless, thickness heterogeneities form before glass transition occurs, and the power-law relation satisfactorily describes viscosity variations during polymer advection. The surface tensions γ of polystyrene solutions in toluene were measured using a tensiometer (Teclis) in a rising bubble configuration. In agreement with data in the literature,[23] we have found that γ slightly increases with volume fraction, ϕ. In the investigated range, the increase is linear: $(\gamma(\phi) - \gamma_0)/\gamma_0 = \Gamma\phi$, where γ_0 is the surface tension of toluene and $\Gamma = 0.06$. Since the increase is very small, in the following we consider that surface tension remains constant during drying $\gamma = \gamma_0 = 27.9$ mN.m^{-1}. We also neglect Marangoni effects in the theoretical analysis, which is later justified in details.

Drying with an evaporation mask

Polymer solutions were spread on clean glass plates (dimensions $100\,mm \times 100\,mm$). Wire-wound rods of different sizes (BYK) were used to obtain liquid films of different initial thicknesses. The resulting thickness depends on the viscosity of the solution but also on the exact volume of solute, which slightly varied from one experiment to another. Therefore, thicknesses of the dried deposits were systematically measured in a region non affected by the evaporation mask, and the initial thicknesses were inferred from both their values and the remaining solvent content at the time of thickness measurements (see the section on the evaporation velocity). Initial thicknesses of the liquid films ranging from 47 μm to 160 μm were obtained with solutions of viscosity ranging from 9 mPa.s to 128 mPa.s. Once the film spread, the glass plate was placed on a dual-axis rotation stage, the horizontality of which was set with an accuracy of 0.05° with a digital inclinometer. The experimental set-up, schemed in figure 2, was installed below a laboratory hood for safety reasons. During drying, the samples were kept in an enclosure covered by a net (commercial mosquito net, mesh size 1.2 mm), ensuring reproducible evaporation conditions. In these conditions, drying is limited by diffusion of solvent in the atmosphere, over a distance close to the one between the surface

of the film and the net, which is 2 cm. A parallelepidic mask, of width $2r = 4.5$ mm along the x-axis defined in figure 2 and of length 100 mm in the direction perpendicular to the plane of the figure, was approached to the surface down to 0.5 mm above the glass plate. The latter distance was chosen because it is much smaller than the vapor diffusion layer, therefore the atmosphere between the mask and the film is expected to be quickly saturated with vapor of solvent. A rotation stage was used to ensure that the lower surface of the mask was parallel to the glass plate.

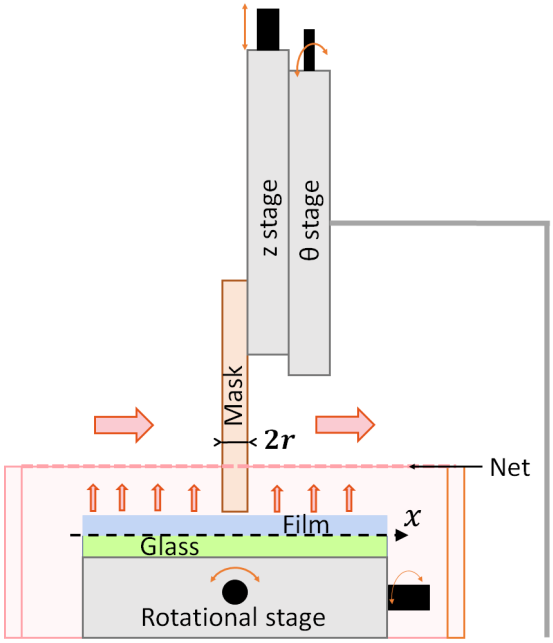

Figure 2: Scheme of the experimental set-up.The glass plate on which the liquid film is spread is placed on a horizontal substrate, within an enclosure covered with a net to reduce air convection.The parallelepipedic evaporation mask is placed at a vertical distance of 0.5mm above the glass surface

Topology measurements and data analysis

Once the film dried, the topography of the sample was measured using a 3D optical surface profiler (Zygo New View 9000). Polymer coating was removed along a line on each sample, in order to obtain a reference value for height measurements. Height profiles were averaged over 30 mm along the transverse direction, perpendicular to the plane of figure 2. An example of

average height profile $h_f(x)$ is shown in figure 3. The masked area, of width $2r$, is represented in grey. The profile is flat away from the mask, showing in particular that edge effects are negligible in the probed region. A depression is observed below the mask, that has a surface area A and is associated with overthicknesses on each side of the mask. We arbitrarily define the width of the thickness heterogeneities resulting from the evaporation mask as the distance between the edge of the mask and the remotest point for which the overthickness with respect to the flat part is 20% of its maximum (see figure 3). Owing to the asymmetry of the experimental profiles, the value of w is averaged on both sides of the mask. Actually, we have found that, unexpectedly, height profiles of the dry deposits were never perfectly symmetric, as a result of both initial heterogeneities of film thickness and residual air flows during drying. Thickness heterogeneities may appear as the glass plate with the spread film is moved to be placed on the stage; in addition, full control of air convection is difficult.

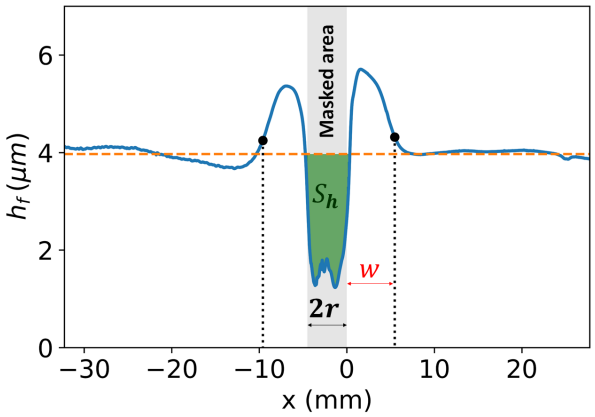

Figure 3: Height profile of a polystyrene layer obtained by drying a thin film of polystyrene in toluene solution of initial volume fraction $\phi_0 = 0.06$ under an evaporation mask of width $2r = 4.5$ mm. A is the surface of the depression caused by the evaporation mask and w the width of the thickness heterogeneities. The origin of the x-axis is chosen at the right edge of the mask, consistently with the notation of figure 5.

Criteria were defined to select only reliable measurements of A and w. First, we checked that the profile was flat far from the mask: we computed the standard deviation of the height in this region and arbitrarily compared it to the third of its average value, i.e. $\bar{h_f}/3$. Second, we ensured that the surface of the depression A was roughly equal to the surface

of the bumps. This is the case if the integral of $h_f - \bar{h_f}$ close to the mask is smaller than a threshold value chosen to be $w\bar{h_f}$. About 70% of the measured profiles met these criteria and the other 30% were discarded.

Evaporation velocity

The evaporation velocity was measured by monitoring the mass variation of a drying liquid film in the same conditions as described above, but without a mask and having replaced the rotation stage by a scale. The mass variations with time of a solution of initial volume fraction $\phi_0 = 0.039$ are shown in figure 4a. As observed in similar systems and evaporating conditions,[24] during a first stage, the mass decreases at an almost constant rate. The evaporation rate decreases down to very small values in a second stage. We define the evaporation velocity $\dot{e} = -dh/dt$ where $h(t)$ is the film thickness at time t. Since evaporation is limited by diffusion of vapour in the atmosphere, the evaporation velocity is therefore given by $\dot{e} = D_v c_{sat}/(\rho\lambda)$ where D_v, c_{sat} and ρ are respectively the diffusion coefficient of vapour in the atmosphere, the concentration in toluene at saturation in the atmosphere and the density of toluene. λ is the length of the diffusion layer above which toluene concentration vanishes because of air advection. From the slope of the red-dotted line in figure 4, the value of the evaporation velocity in the first stage is $\dot{e} = 3 \times 10^{-7}$ m.s^{-1}. With $c_{sat} = 0.14$ kg.m^{-3},[25] $D_v = 8 \times 10^{-6}$ m^2.s^{-1},[26] and $\rho = 870$ kg.m^{-3}, we obtain $\lambda = 0.3$ cm. This value is smaller than the value of the vertical distance between the film surface and the mosquito net in the experimental set-up, which indicates that convective effects may be at stake under the net. Nevertheless, the value of the evaporation velocity was found to be reproducible. As evaporation proceeds, the activity and thus the saturation concentration decreases with decreasing toluene content in the film. This decrease is described by a Flory-Huggins sorption isotherm with a Flory parameter of 0.4.[27] We have checked that the decrease of the evaporation velocity in the second stage could be entirely attributed to the decrease of solvent activity; in particular, it does not result from the formation of a concentrated skin, as reported during

the evaporation of thick films of polymer solutions.[28]

Additional information is reported in figure 4b in which the mean polymer volume fraction deduced from the mass curve is shown as a function of the dimensionless time $T = t\dot{e}_\infty/h_0$, where $\dot{e}_\infty$ is the evaporation rate, the index ∞ indicating that the value is the one far from the mask, and h_0 the initial thickness of the film. It is compared to the volume fraction computed by assuming a constant evaporation velocity. In the considered experiment, the two curves sumperimpose for normalised times up to $T \simeq 0.6$, far from glass transition, and at that time the viscosity of the polymer solution is about twenty times its initial value. We emphasise that the maximum value of T, which corresponds to the time at which $\phi = 1$, is smaller than unity since polymer does not evaporate. More precisely the maximum value of T - in the approximation where the evaporation rate is constant - is given by $\left(1 - \frac{\phi_0}{\phi_{end}}\right)$ where ϕ_{end} is the volume fraction at which the experiment is ended, i.e. at which the thickness measurements are performed. Film thicknesses were always measured between 30 minutes and 3 hours after the beginning of drying. The value of ϕ_{end} can be extrapolated from the data of figure 4, in which the volume fraction is observed to increase linearly with time in the stage following the evaporation at a constant rate. We have found that the polymer volume fraction ϕ_{end} ranged from 0.72 to 1 at the times the thicknesses were measured. The latter values were used first to compute the initial film thickness - and its uncertainty - from the measured one, and second to determine the final time T, which average value was found to be 0.9.

Results and Discussion

Theoretical analysis

The evaporation mask creates a step of evaporation flux, which generates steps of both film thickness and polymer concentration, and the resulting flows are responsible for the final shape of the dry film. In the present section, we develop an analytical approach based on

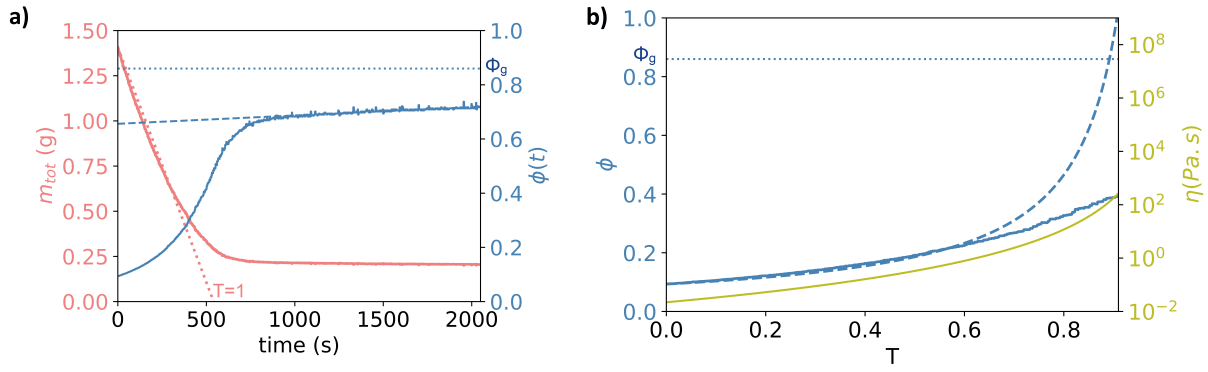

Figure 4: (a) Measured mass (pink line, left axis) and polymer volume fraction, averaged over the whole surfacea area and deduced from the mass curve (blue line, right axis) of a thin film of polystyrene in toluene solution as a function of time. The initial volume fraction is $\phi_0 = 0.09$. The pink dotted line corresponds to a constant evaporation rate of $\dot{e}_\infty = 3 \times 10^{-7} m.s^{-1}$ and crosses the horizontal axis at a dimensionless time $T = t\dot{e}_\infty/h_0 = 1$. The blue dotted line indicates the glass transition volume fraction ϕ_g. The blue dashed line shows the slow linear increase of volume fraction at larger times. (b) (left axis) Volume fraction as a function of the dimensionless time T, measured (full blue line, same data as (a)) and computed by assuming a constant evaporation velocity (dotted line). (right axis) Viscosity variations with T of the polymer solution inferred from the measured volume fraction and using $\eta = \eta_{ref}\phi^\nu$ (green line).

linearised flow equations that account for the viscosity increase during drying. Our aim is to predict the variations of the extent and amplitude of the final thickness heterogeneities with the controlled parameters, namely the initial film thickness and viscosity, and the evaporation velocity.

Hypotheses

As schemed in figure 5, we consider a 2D liquid film of initial thickness h_0 and initial volume fraction in solute ϕ_0. The film is assumed to be infinite along the horizontal x-axis. For the sake of simplicity, only one edge of the evaporation mask is considered. The film thickness is denoted $h(x,t)$. The hypotheses of the model are the following: (i) The evaporation velocity $\dot{e}$ is zero below the mask (for $x < 0$) and has a constant value $\dot{e}_\infty$ everywhere else (for $x > 0$). It writes $\dot{e}(x) = \dot{e}_\infty \Theta(x)$, where Θ is the Heaviside function

(ii) The Péclet number in the vertical direction, given by $Pe_v = \dot{e}_\infty h_0/D$, where D is

the mutual diffusion coefficient, is assumed to be very small. As a result, the solute volume fraction in the vertical direction remains homogeneous.

(iii) The Péclet number in the horizontal direction, given by $Pe_h = u_x\ x^\star/D$ where u_x is the horizontal velocity in the liquid layer and x^* the lateral length scale, is assumed to be very large; diffusion along the x-axis is therefore negligible.

(iv) Marangoni flows are negligible. The surface tension is in particular considered to be constant and equal to the one of pure solvent, γ_0. Consequently, the boundary condition for the flow at the free surface of the film is a zero-stress condition.

(v) The liquid viscosity is space-independent but time-dependent, and denoted $\eta(t)$. Viscosity increases with time because the concentration in solute increases in the evaporating film.

The relevance of these assumptions with respect to the experimental conditions will be discussed at the beginning of the last section that compares experimental and theoretical data.

Equation for film thickness

We now establish the equation describing the variations of the film thickness $h(x,t)$ and further linearize it, by writing thickness variations as perturbations to a reference state. The reference state can either be chosen far from the mask, where the film evaporates at a constant rate, or under the mask where no evaporation occurs. We will see in the following that the same formalism can be used whatever the reference state. In a first stage, we consider the reference that is away from the mask, hence the reference thickness and volume fraction are respectively $h_\infty(t) = h_0 - \dot{e}_\infty t = h_0(1-T)$ and $\phi_\infty = \phi_0\left(\frac{1}{1-T}\right)$, where T is the dimensionless time introduced above.

Since the film thickness is much smaller than its horizontal dimensions, the flow is described by the Navier-Stokes equation in the lubrication approximation. The latter equation is further integrated with the relevant boundary conditions, i.e. vanishing velocity at the

glass/liquid interface and zero-stress at the air/liquid interface, yielding[13]

$$\frac{\partial h}{\partial t} - \frac{1}{3\eta(t)}\frac{\partial}{\partial x}\left(h^3\frac{\partial p}{\partial x}\right) = -\dot{e}(x) \tag{1}$$

where $p(x,t)$ is the pressure in the liquid film. The pressure at a given height in the film is the sum of the hydrostatic pressure and the Laplace pressure. Therefore, its gradient can be written simply as $\partial_x p(x,t) = \rho g \partial_x h - \partial_x\left(\gamma \partial_{xx} h\right)$ where the first term of the r.h.s. is the hydrostatic pressure gradient and the second term corresponds to capillary pressure.

We further linearize equation 1 by writing that $h(x,t) = h_\infty(t) + h_0\delta(x,t)$ where $h_\infty(t)$ is the reference thickness and the dimensionsless perturbation $|\delta(x,t)|$ is assumed to be smaller than $1 - T$.

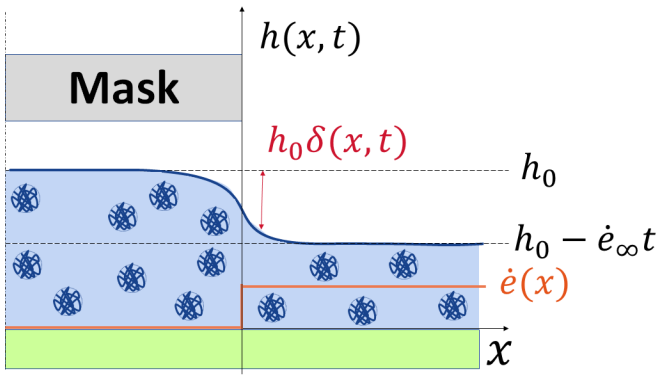

Figure 5: Schematical representation of the problem. The thickness variations resulting from the presence of the evaporation mask are considered as perturbations to a reference state (here, the evaporating film far from the mask).

Three velocities can be defined in the considered system, namely:

(i) the evaporation velocity $\dot{e}_\infty$ which is of the order of $3.10^{-7}\mathrm{m.s}^{-1}$

(ii) The capillary velocity $V_c(t) = \frac{\gamma_0}{\eta_0}$. In the considered problem, $V_c \simeq 1\mathrm{m.s}^{-1}$

(iii) the gravitational velocity $V_g = \frac{\rho g h_0^2}{\eta_0}$. This velocity is the run-off velocity of a liquid film of thickness h_0 on a vertical wall under the action of gravity. Its value is 4 $\mathrm{mm.}s^{-1}$ for a thickness of 100 µm. Equation 1 is linearised and expressed using the above velocities, yielding

$$\frac{\partial \delta}{\partial t} - S_d \left(V_g h_0 \frac{\partial^2 \delta}{\partial x^2} - V_c h_0^3 \frac{\partial^4 \delta}{\partial x^4} \right) = \frac{\dot{e}_\infty}{h_0}(1 - \Theta(x)) \tag{2}$$

where we have introduced the dimensionless slowing down factor S_d that accounts for the time variations of both liquid viscosity and film thickness far from the mask, and is given by

$$S_d = \frac{{h_\infty}^3(t)}{3h_0^3} \frac{\eta_0}{\eta(t)} \tag{3}$$

We emphasise that the viscosity is assumed to be homogeneous and equal to the one of the drying film far from the mask. Both the increase of viscosity and the thinning of the film are responsible for the slowing down of the flow. In contrast, if the reference state is chosen under the mask where no evaporation occurs, the height remains constant as well as the viscosity, corresponding to a constant slowing down factor S_d. Using the power law variation of viscosity $\eta = \eta_0 \left(\phi/\phi_0\right)^\nu$ together with relation $\phi = \phi_0 h_0/h_\infty$ to express $\eta(T)$, the slowing down factor defined in equation 3 can be written as

$$S_d = \frac{(1-T)^\alpha}{3} \tag{4}$$

where the exponent is $\alpha = 3 + \nu$ for a reference state chosen far from the mask. For a reference state under the mask, equation 3 becomes simply $S_d = 1/3$, which corresponds to an exponent $\alpha = 0$. The use of exponent α therefore makes equation 4 general, whatever the reference state that is chosen. Finally, we introduce a dimensionless effective time τ that takes into account the slowing down process

$$\tau(T) = \int_0^T S_d(T')dT' \tag{5}$$

The effective time corresponds to the time that would elapse in a film of constant viscosity and thickness with an equivalent flow. If S_d decreases with time, τ varies sublinearly with time, reflecting the slowing down of the flow in the film induced both the viscosity increase

and the thinning of the film. After integration, equation 5 becomes

$$\tau(T) = \frac{1}{3\,(1+\alpha)}\left(1-(1-T)^{1+\alpha}\right) \tag{6}$$

Now that we have determined the time scale of the problem, we turn to the length scales. The vertical length scale is given by the initial thickness and we use $h_0\delta$ as vertical perturbation. Choice of the lateral length scale depends on the effect driving the flow. If the flow is governed by capillarity, making equation 2 dimensionless in x, as shown below, gives the lateral length scale of the perturbation

$$x_c^\star = h_0\left(\frac{V_c}{\dot{e}_\infty}\right)^{1/4} \tag{7}$$

The same length x_c^* has been introduced in previous works on the non uniform drying of thin films of colloidal suspensions.[13,14] Actually, it has been identified as the length at which the flow caused by evaporation is balanced by the flow resulting from capillarity. Introducing the dimensionless variable $\xi_c = x/x_c^*$, equation 2 becomes in the limit of dominant capillarity

$$\frac{\partial\delta}{\partial\tau} + \frac{\partial^4\delta}{\partial\xi_c^4} + O(H) = \frac{1-\Theta(\xi_c)}{S_d(\tau)} \tag{8}$$

where

$$H = \frac{V_g}{V_c^{1/2}\dot{e}_\infty^{1/2}} \tag{9}$$

In contrast, when gravity dominates, the perturbation extends over a length scale

$$x_g^* = h_0\left(\frac{V_g}{\dot{e}_\infty}\right)^{1/2} \tag{10}$$

Using the dimensionless variable $\xi_g = x/x_g^*$, equation 2 becomes

$$\frac{\partial\delta}{\partial\tau} - \frac{\partial^2\delta}{\partial\xi_g^2} + O(1/H^2) = \frac{1-\Theta(\xi_g)}{S_d(\tau)} \tag{11}$$

The crossover between capillarity and gravity dominated regimes is given by $H = 1$ which corresponds to $V_g = \sqrt{V_c \dot{e}_\infty}$. H is proportionnal to h_0 and can be expressed as $H = h_0/h^{CO}$, where h^{CO} is the crossover thickness between capillary and gravity dominated regime given by

$$h^{CO} = \frac{(\eta_0 \gamma_0 \dot{e}_\infty)^{1/4}}{(\rho g)^{1/2}} \tag{12}$$

If $h_0 \gg h^{CO}$, then $H \gg 1$ and gravity effects are much larger than capillary ones. The height of the liquid under the mask then relaxes under the action of gravity with a characteristic lateral length scale given by $x_g^\star$. In contrast, if $h_0 \ll h^{CO}$, flows are induced by capillarity and the width of the resulting thickness heterogeneities are related to $x_c^\star$. The crossover between the two regimes - for $H = 1$- corresponds not only to equal characteristic lengths for capillarity and gravity, but also to their equality with the capillary length, $x_g^\star = x_c^\star = l_c = \sqrt{\gamma_0/\rho g}$. The qualitative variations of the horizontal length scale as a function of the film initial thickness are shown in figure 6. The length scale varies with thickness as a power law, with an exponent that depends on the governing effect: it is proportional to h_0 for governing capillarity and to h_0^2 for governing gravity. The horizontal axis can also be represented as a runoff velocity axis since V_g varies with h_0^2. A critical velocity V_g^c is associated with the critical height that delimits the two regimes. The same two length scales that are determined by the latter analysis can also be found from the initial non-linearised equations, as shown in the Supporting Information. Although crude, the approximation we use nonetheless provides the same variation laws of the characteristic lengths as the non approximated equations.These variation laws can be expressed under the general form $x^* \propto l_c(h_0/h^{CO})^n$ with respectively $n = 1$ for prevailing capillarity and $n = 2$ for leading gravity.

Table 1 gathers the different characteristic velocities and lengths and their expected numerical values. We emphasise the critical height h^{CO} is one order of magnitude smaller than the capillary length. Therefore, gravity can drive the relaxation of liquid films subjected

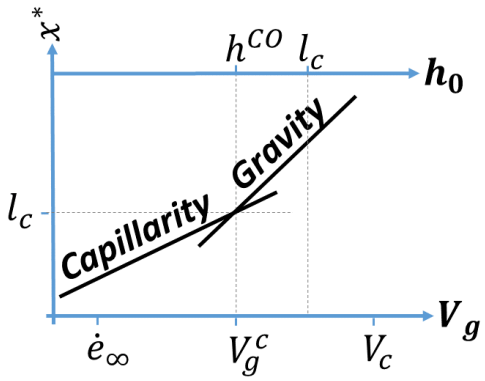

Figure 6: Characteristic lateral length scales given by equations 7 and 10 of the perturbation versus run-off gravity velocity, or thickness of the initial coating.

to nonuniform evaporation, even when their thicknesses are much smaller than the capillary length. Consistently, the non negligible role of gravity has been evidenced in the kinetics of drying fronts in films of colloidal suspensions.[14]

Table 1: Table of the various velocities and lengths

Name	Symbol	Expression	Typical Value
Initial thickness	h_0		100 µm
Surface tension	γ_0		3.10^{-2} N.m^{-1}
Viscosity	η_0		2.10^{-2} Pa.s
Capillary length	l_c	$(\frac{\gamma_0}{\rho g})^{1/2}$	1.8 mm
Drying velocity	$\dot{e}_\infty$	$-\frac{dh_\infty}{dt}$	3.10^{-7} m.s^{-1}
Capillary velocity	V_c	$\frac{\gamma_0}{\eta_0}$	1 m.s^{-1}
Gravity run-off velocity	V_g	$\frac{\rho g h_0^2}{\eta_0}$	4.10^{-3} m.s^{-1}
Cross-over thickness	h^{CO}	$l_c \left(\frac{\dot{e}_\infty}{v_c}\right)^{1/4}$	40 µm
Capillary lateral extent	$x_c^\star$	$h_0 \left(\frac{v_c}{\dot{e}_\infty}\right)^{1/4}$	5 mm
Gravity lateral extent	$x_g^\star$	$h_0 \left(\frac{v_g}{\dot{e}_\infty}\right)^{1/2}$	1 cm

Analytical solutions

We first focus on the case of governing gravity. Equation 11 is analogous to a diffusion equation with a source term. The solution to a diffusion equation with a forcing term that is the product of a spatial Heaviside function by a Dirac function (step applied at $t = 0$) is an error function erf. Therefore, in the considered limit, the solution to equation 11 is the

convolution of the error function and S_d with the boundary conditions $\delta(\xi_g = +\infty) = 0$ and $\delta(\xi_g = -\infty) = \dot{e}_\infty t$, if the reference situation is the one outside the mask. Changing the time variable to the dimensionless time $T = \dot{e}_\infty / h_0 t$ and using the derivative of equation 5 to get $d\tau/dT = S_d$, one obtains

$$\delta(\xi_g, T) = \frac{1}{2} \int_0^T \left(1 - \mathrm{erf} \left(\frac{\xi_g}{2\sqrt{\tau(T) - \tau(T')}} \right) \right) dT' \tag{13}$$

In contrast, when capillarity prevails, i.e. $H \ll 1$, the solution to equation 8 can be deduced from the analytical solution derived by Salez *et al* for the height relaxation of a nonevaporating thin film following an initial step-like height at time $t = 0$.[29] The action of capillarity only was considered in the latter problem, and the corresponding equation has the same left hand side as equation 8. The solution is a function χ that can be expressed with (1,3)-generalized hypergeometric functions given in the Suporting Information as the solution to the capillary case. The solution to equation 8 can thus be expressed as an integral of the χ solution, using $\delta(\xi_c = +\infty) = 0$ and $\delta(\xi_g = -\infty) = \dot{e}_\infty t$ as a boundary condition, yielding

$$\delta(\xi_c, T) = \frac{1}{2} \int_0^T \left(1 - \chi \left(\frac{\xi_c}{(\tau(T) - \tau(T'))^{1/4}} \right) \right) dT' \tag{14}$$

Resulting thickness profiles of the film are shown at different times in the supporting information. In the next section, we focus on the polymer thickness inferred from the results of the present section.

Polymer thickness

The film thickness $h(x, t)$ is obtained from equation 13 when gravity is at stake and equation 14 when it is capillarity. Up to this point we have considered a time dependent but space independent polymer volume fraction ϕ but, since the polymer is advected by the flow, its volume fraction is a function of both time and position. We show that it can be determined

through conservation equations. We now consider the polymer volume per surface unit in the film, $\sigma(x,t) = h(x,t)\phi(x,t)$ which corresponds to the polymer thickness at position x if solvent was removed at time t without displacing the polymer. At long times, for vanishing solvent content, it tends towards the thickness of the dried layer. A simple relation can be found between σ and δ by writing the conservation equations of both solvent and polymer. Its full derivation is detailed in the Supporting Information and the qualitative argument is the following: The polymer is advected by the flow and, in the frame of the linear approximation, its concentration under the mask remains constant. As a result, the default or excess of liquid respectively under and outside the mask corresponds to the default of thickness with respect to h_0 for $x < 0$ and the excess for $x > 0$ with respect to $h_0 - \dot{e}_\infty t$ outside the mask. The corresponding relation between σ and δ is

$$\sigma(x,t) = \sigma_0 \left[1 + \delta - (1 - \Theta(x))\frac{\dot{e}_\infty}{h_0}t\right] \tag{15}$$

where $\sigma_0 = h_0\phi_0$ is the initial value of σ.

The profiles of σ are shown at different times in figure 7 and as a function of the normalised coordinates, respectively $x/x_c^\star$ and $x/x_g^\star$ in the capillarity and gravity driven regimes. The profiles have similar shapes in both regimes: as expected, they exhibit a depression under the mask and an overthickness close to its edge in the evaporating film. Further away from the edge, non monotonic variations occur for dominant capillarity, whereas the profiles are flat when gravity prevails. In the capillarity-driven regime, the profiles are similar to the ones obtained in the same regime by the numerical resolution of Routh and Russel[13] for a constant viscosity.

The amplitudes of σ are similar in both regimes, but the lateral extents differ in the normalised representation of figure 7. Dominant capillarity results in wider thickness heterogeneities with respect to the relevant length scale. The length scales $x_c^\star$ and $x_g^\star$ themselves differ, and in particular vary differently with the initial film thickness. In order to compare the analytical results to the experimental ones, we have defined the same lateral extents w

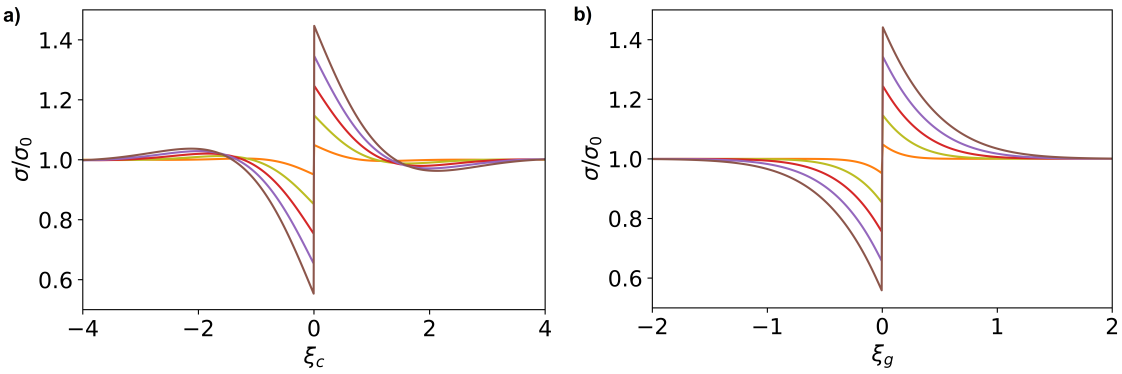

Figure 7: Normalised polymer height in the capillarity-driven regime as a function of ξ_c (a) and in the gravity-driven regime as a function of ξ_g (b) at different normalised times: $T = 0.1$(orange), $T = 0.3$ (green), $T = 0.5$(red), $T = 0.7$ (purple) and $T = 0.91$ (brown). The polymer height was computed using equation 15 and respectively equations14 and 13 and with a reference state under the mask, i.e. $\alpha = 0$.

of the profiles as in the experiments, which correspond to an overthickness of 0.2 times its maximum value, i.e. $\sigma(w) - \sigma_0 = 0.2\,(\sigma_{max} - \sigma_0)$. The extents, normalised by the relevant length scale x^*, are shown as a function of the dimensionless time T in figure 8. They both vary with time in a non monotonic fashion for a reference stage far from the mask corresponding to $\alpha = 3 + \nu$. In contrast, the extents for the reference state taken under the mask ($\alpha = 0$), grow monotonically in both gravity and capillarity-driven regimes.

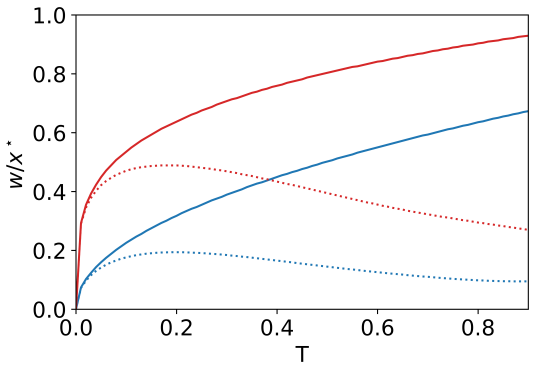

Figure 8: Lateral extent of the thickness heterogeneity normalized by the characteristic length scale $x^\star$ of the corresponding regime as a function of the normalised time T in the capillarity (red lines) and gravity-driven (blue lines) limits. The curves correspond to different reference states for linearization: under the mask $\alpha = 0$ (full lines) and away from the mask $\alpha = \nu + 3$ (dotted lines)

The surface area A characterising the amplitude of thickness heterogeneities can be ob-

tained by integration of σ over $x > 0$ (or equivalently for $x < 0$, the profiles being symmetric), yielding the general expression

$$A = 2\beta(\alpha, T)x^* h_0 \phi_0 \tag{16}$$

The prefactor β is a numerical factor that depends only on α and on T. Its expression for prevailing gravity is

$$\beta_g = \frac{\int_0^T \left(\sqrt{\tau(T) - \tau(T')}\right) dT'}{\sqrt{\pi}} \tag{17}$$

For prevailing capillarity the spatial integration of equation 14, is detailed in the Supporting Information. It yields the following expression for the prefactor

$$\beta_c \simeq 0.39 \int_0^T \left(\tau(T) - \tau(T')\right)^{1/4} dT' \tag{18}$$

We emphasise that the dependency of the prefactors on α results from the dependency of the dimensionsless time $\tau(T)$ on the chosen reference state, as established in equation 6. The variations of β with T are shown in figure 9 for both regimes and both reference states. As expected, the prefactors, and thus the surfaces of the formed depression grow with time and are not only larger but also keep increasing later for a reference state chosen under the mask

.

The expression of the surface of the depression can be put under a more generalised form by using the cross over thickness given by equation 12 and, in the following, we will use the expression

$$A = \phi_0 l_c^2 \left(\frac{h_0}{h^{CO}}\right)^{n+1} \beta(T, \alpha) \left(\frac{\dot{e}_\infty}{V_c}\right)^{1/4} \tag{19}$$

where the exponent n is 2 in the gravity-driven regime and 1 when capillarity prevails, and the prefactor β is given either by equation 17 or 18.

In summary, we have used a linear approximation in order to solve the flow equations in regimes driven by either gravity or capillarity. The obtained analytical expressions of the

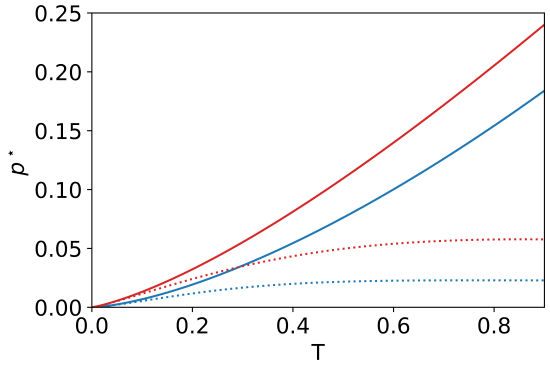

Figure 9: Prefactor of the surface area of the formed depression (as defined in equation 16) as a function of the normalised time T in the capillarity (red lines) and gravity-driven (blue lines) regimes, given respectively by equations 18 and 17. Solution for both reference states (under the mask (full lines) and far from it (dotted lines)) are shown.

height of the film allow computation of the polymer thickness at each instant. We have found that the pattern resulting from the advection of solute during drying varies with time. The lateral extent and the amplitude of the formed pattern as defined in figure 3) vary with the different parameters following $w \propto l_c(h_0/h^{CO})^n$ and $A \propto \phi_0 l_c^2(h_0/h^{CO})^{n+1}(\dot{e}_\infty/V_c)^{1/4}$ with respectively $n = 1$ for prevailing the capillarity and $n = 2$ for leading gravity. The choice of the reference state selects the values of the time varying prefactors for both extent and amplitude. In the next section, these predictions are compared to experimental results but we first discuss the relevance of the hypotheses made in the preceding analysis, with respect to the experimental conditions.

Comparison to experimental results

Justification of the neglected effects

The first assumption made in the model presented above is that the evaporation velocity does not vary with time. In the example shown, corresponding to a volume fraction $\phi_0 = 0.09$, the curves superimpose up to a normalised time $T = 0.6$. At later times, the evaporation velocity is smaller in the experiment since the activity of toluene decreases. However, the decrease in evaporation rate is limited to about 20% between $T = 0.6$ and $T = 1$. Since the extent and

amplitude of the thickness heterogeneities vary at most with $\dot{e}_\infty^{1/2}$, the error resulting from the overestimation of the evaporation rate is therefore small. In contrast, the error made on the polymer volume fraction and thus on the liquid viscosity is significant, as shown in figure 4b. However, we will see below that the experimental data is well accounted for with a reference state under the mask, where the viscosity does not vary. Hence, the assumption of a constant evaporation velocity is fully relevant for the description of experimental data. Note that the analytical results used in the next section will all be presented using $T = 0.9$ that corresponds roughly to the maximum value of T of our experiments.

The second and third assumptions concern the vertical and horizontal Péclet numbers: diffusion is assumed to be large enough for the film to remain homogeneous in the vertical direction whereas lateral diffusion is neglected. The Péclet number in the vertical direction is $Pe_v = \dot{e}_\infty h_0/D$ where D is the mutual diffusion coefficient. Since thickness heterogeneities form before glass transition, D remains close to $D = 10^{-10}$ $\mathbf{m^2.s^{-1}}$, as measured in polystyrene solutions in toluene of similar molar mass.[21] As a result, Pe_v remains smaller than unity, and the solution can be considered as homogeneous in the vertical direction. The horizontal Péclet number is $Pe_h = u_x\ x^\star/D$ where u_x is the horizontal velocity. For prevailing gravity, an estimate of the horizontal velocity is obtained from the thin-film equation, yielding $u_x \simeq V_g h_0/x^\star$. The resulting Péclet number is larger than 10^3 and lateral diffusion can safely be neglected.

In a fourth assumption, we have neglected any Marangoni effect. Both thermal and solutal Marangoni flows can arise during drying and may modify the effect of an evaporation mask.[30] Since no evaporation occurs under the mask, the temperature of the surface under the mask is larger than in the regions where evaporation takes place. A flow directed toward the coldest regions, away from the mask, is therefore expected. Similarly, since the surface tension of polystyrene solutions increases with increasing polymer content a solutal Marangoni flow is created in the same direction. We emphasise these two effects are of second order in δ and thus non-linear; estimates of their magnitudes are therefore difficult to provide.

Nevertheless thermal and solutal Marangoni numbers can be defined by $Ma = \partial_x\gamma/(h\partial_x P)$. When gravity drives the flows and for $h = 100$ μm and $x^\star = 1\,$cm, the denominator is of the order of $h_0^2\rho g/x^\star \simeq 10^{-2}\ Pa$. The temperature difference is at most a few K - as measured with an IR camera - and the derivative of surface tension with respect to temperature is $\partial_\theta\gamma \simeq 10^{-4}$ Pa,[24] yielding $\partial_x\gamma \simeq 10^{-2}$ and $Ma \simeq 1$. The solutal Marangoni effect is larger: Despite the small variations of surface tension with solute concentration of the chosen solution, $\partial_x\gamma$ is of the order of $\gamma_0\Gamma/x^\star \simeq 1\ Pa$, where Γ is the maximum relative variation of surface tension between the beginning and the end of the drying. The corresponding Marangoni number is $Ma \simeq 10$. We have performed additional numerical resolution of the gravity-driven flow equations to measure the effect of Marangoni numbers larger than unity on the width of the thickness heterogeneities w. We have found that it remained negligible for a Marangoni number of 10. Consistently, we show in the following that the experimental data agree with the predicted ones without accounting for Marangoni effects. The latter would however need to be considered in the case of aqueous polymer solutions, the surface tensions of which generally strongly depend on concentration.

Finally, the spatial variations of viscosity are neglected, which is obviously a strong approximation under the mask, where there is no evaporation and thus no viscosity increase. However this assumption is required to solve the problem analytically. As a result, we expect the theoretical predictions to underestimate the dimensions of the formed patterns when the reference state is chosen far from the mask and, in contrast, to overestimate them when the reference state is under the mask. Using the same formalism, we are able to provide an upper and lower bound for the amplitude and lateral extent of the formed pattern. We compare the experimental results to this prediction in the next section.

Width and amplitude of thickness heterogeneities

Experiments were performed at different initial polymer volume fractions, yielding films with different viscosities and initial thicknesses, which are therefore the experimental parameters. We first report the experimental extent of thickness heterogeneities, which is shown in

figure 10 together with theoretical data. The raw data is displayed in the inset. Widths ranging from a few millimetres to a few centimetres were measured on the sample, whereas initial thicknesses are in the range of hundreds of microns, i.e. about a hundred times smaller. The width of the region affected by the nonuniform evaporation can therefore be larger than the size of the evaporation heterogeneity, here set by the 4.5 mm-wide mask. The main figure shows the normalised data, respectively by the capillary length on the y-axis and by the critical thickness given by equation 12 on the x-axis. The adopted representation allows to compare experimental data obtained with different initial volume fractions with theoretical data corresponding to the different regimes. The theoretical curves are given for the two reference states, corresponding respectively to a reference state from the mask, where the flow is strongly slowed down, and under the mask where the flow does not slow down. We have checked that, for both references states, the mask is wide enough to neglect mutual influence between both sides. As expected, the results obtained with the first reference state underestimate the experimental data. In contrast, we observe that they are quantitatively described when no slowing down is accounted for and, in addition, that they lie in the range of prevailing gravity.

A similar agreement is found for the amplitudes of the depression of the dry deposit. Figure 11 shows the measured surface area A as a function of the ratio of the initial thickness and the crossover thickness. In the main figure, the surface is normalised by square of the capillary length, the initial volume fraction and $(\dot{e}_\infty/V_c)^{1/4}$. As observed for the extent w, the agreement between experimental and theoretical findings is very good, in the frame of the linear approximation with a reference state under the mask. The data are therefore well described with the simplest approach, which considers that the viscosity keeps its initial value. Furthermore, the simplified step-like vapor concentration we have used well accounts for the real vapor concentration above the film.

In summary, in our experimental conditions, we have shown that gravity always prevails and that the linear approximation made with a reference state under the mask allows an

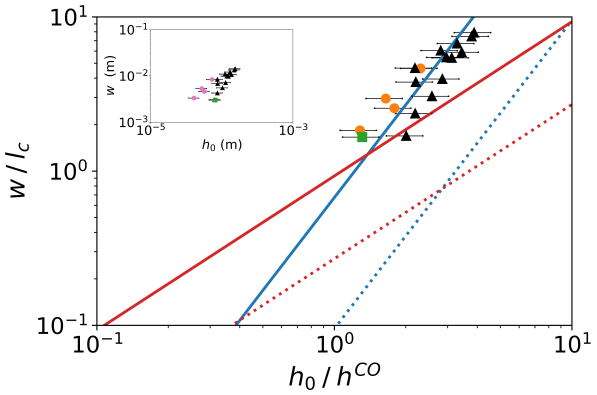

Figure 10: Lateral extent w of the thickness heterogeneities normalised by the capillary length l_c as a function of the normalized initial thickness h_0/h^{CO}, with h^{CO} given by equation 12. The theoretical predictions are shown for prevailing capillarity (red lines) and gravity (blue lines), that were respectively computed for a reference state under the mask (full lines) and far from the mask (dotted lines). They correspond to a drying time $T = 0.9$ The experimental data were obtained with different values of initial polymer volume fraction ϕ_0: 0.06 (orange circles), 0.09 (black triangles) and 0.17 (green squares). Inset: raw data. The horizontal error bars result from the uncertainty on the initial thickness.

excellent prediction of the features of the dried film.

The agreement between experimental and theoretical data in particular validates the variation laws we have obtained for the extent and amplitude according to the different parameters. We emphasise the features of the formed pattern exhibit a strong dependence on the initial film thickness, which is therefore the key parameter to control the pattern resulting from a region where evaporation is blocked. Interestingly, when the evaporation mask is replaced by a nozzle in which a carrier gas is blown, the width and amplitude of the thickness heterogeneities have been reported to first increase with film thickness and then reach a plateau,[20] in the same thickness range as the one investigated here. It demonstrates that controlling the nonuniformity of evaporation fluxes offers a way to tune the deformations of the final dry layer but also to change the key parameters that control the deformation.

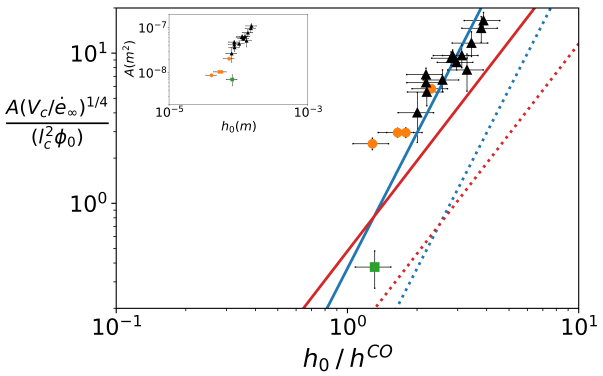

Figure 11: Surface area of the normalised depression A as a function of the thickness ratio h_0/h^{CO}. Inset: raw data. Same symbols and horizontal error bars as in figure 10. The vertical error bars correspond to the experimental uncertainty on the thickness of the flat part of the film.

Conclusions

We have presented a quantitative comparison of the thickness heterogeneities of films of polymer solutions resulting from a controlled heterogeneous evaporation flux. We have considered the lateral flows in a thin film induced by the presence of an evaporation mask and driven either by capillarity or gravity, and we have shown that, in each regime, the thickness of the film during drying could be analytically expressed by solving linearised thin film equations. We have thus evidenced the leading role of gravity in films whose thicknesses are down to one order of magnitude smaller than the capillary length. We have further determined the scaling laws verified by the dimensions of the pattern formed by polymer accumulation during drying. The agreement with experiments performed with polystyrene solutions in toluene is very good, demonstrating the relevance of our approach. We have found that the extents of thickness heterogeneities strongly depend on the initial film thickness, whereas they only weakly vary with the physical properties of the solution and the evaporation rate. These results are of particular interest for liquid coating applications that require spatial uniformity of the dried layer. More generally, they shed new light on the accumulation effects associated with drying of complex fluids.

Acknowledgement

We gratefully acknowledge Martin Maza-Cuello for his help in the numerical resolution of the thin-film equation with a Marangoni term.

Supporting Information Available

- Derivation of the linearised equations
  - Solution for the capillary case
  - Relation between σ and δ
  - Characteristic length scales by making the non-linearised equation dimensionless
  - Figures of the computed film thickness $h(x,t)$ as a function of x and at different times for either prevailing gravity or capillarity and a reference state chosen either under the mask or outside the mask.

References

(1) Deegan, R.; Bakajin, O.; Dupont, T.; Huber, G.; Nagel, S.; Witten, T. Capillary flow as the cause of ring stains from dried liquid drops. *NATURE* **1997**, *389*, 827–829.

(2) Kajiya, T.; Monteux, C.; Narita, T.; Lequeux, F.; Doi, M. Contact-Line Recession Leaving a Macroscopic Polymer Film in the Drying Droplets of Water-Poly(N, N-dimethylacrylamide) (PDMA) Solution. *Langmuir* **2009**, *25*, 6934–6939.

(3) Fischer, B. J. Particle convection in an evaporating colloidal droplet. *Langmuir* **2002**, *18*, 60–67.

(4) Boulogne, F.; Ingremeau, F.; Stone, H. A. Coffee-stain growth dynamics on dry and wet surfaces. *Journal of Physics: Condensed Matter* **2016**, *29*, 074001.

(5) Erbil, H. Y. Control of stain geometry by drop evaporation of surfactant containing dispersions. *Advances in colloid and interface science* **2015**, *222*, 275–290.

(6) Brutin, D.; Sefiane, K. *Drying of Complex Fluid Drops: Fundamentals and Applications*; Royal Society of Chemistry, 2022; Vol. 14.

(7) Kajiya, T.; Kobayashi, W.; Okuzono, T.; Doi, M. Controlling the drying and film formation processes of polymer solution droplets with addition of small amount of surfactants. *The Journal of Physical Chemistry B* **2009**, *113*, 15460–15466.

(8) Kim, H.; Boulogne, F.; Um, E.; Jacobi, I.; Button, E.; Stone, H. A. Controlled uniform coating from the interplay of Marangoni flows and surface-adsorbed macromolecules. *Physical review letters* **2016**, *116*, 124501.

(9) Larson, R. G. Transport and deposition patterns in drying sessile droplets. *AIChE Journal* **2014**, *60*, 1538–1571.

(10) Routh, A. F. Drying of thin colloidal films. *Reports on Progress in Physics* **2013**, *76*, 046603.

(11) Hwa, J. C. Mechanism of film formation from latices. Phenomenon of flocculation. *Journal of Polymer Science Part A: General Papers* **1964**, *2*, 785–796.

(12) Okubo, M.; Takeya, T.; Tsutsumi, Y.; Kadooka, T.; Matsumoto, T. Asymmetric porous emulsion film. *Journal of Polymer Science: Polymer Chemistry Edition* **1981**, *19*, 1–8.

(13) Routh, A. F.; Russel, W. B. Horizontal drying fronts during solvent evaporation from latex films. *AIChE Journal* **1998**, *44*, 2088–2098.

(14) Nassar, M.; Gromer, A.; Favier, D.; Thalmann, F.; Hébraud, P.; Holl, Y. Horizontal drying fronts in films of colloidal dispersions: influence of hydrostatic pressure and collective diffusion. *Soft Matter* **2017**, *13*, 9162–9173.

(15) Nassar, M.; Gromer, A.; Thalmann, F.; Hébraud, P.; Holl, Y. Velocity of lateral drying fronts in film formation by drying of colloidal dispersions. A 2D simulation. *Journal of Colloid and Interface Science* **2018**, *511*, 424–433.

(16) Harris, D. J.; Hu, H.; Conrad, J. C.; Lewis, J. A. Patterning colloidal films via evaporative lithography. *Physical review letters* **2007**, *98*, 148301.

(17) Kolegov, K.; Barash, L. Y. Applying droplets and films in evaporative lithography. *Advances in Colloid and Interface Science* **2020**, *285*, 102271.

(18) Parneix, C.; Vandoolaeghe, P.; Nikolayev, V. S.; Quéré, D.; Li, J.; Cabane, B. Dips and Rims in Dried Colloidal Films. *Physical Review Letters* **2010**, *105*, 266103.

(19) Vieyra Salas, J. A.; van der Veen, J. M.; Michels, J. J.; Darhuber, A. A. Active Control of Evaporative Solution Deposition by Modulated Infrared Illumination. *The Journal of Physical Chemistry C* **2012**, *116*, 12038–12047.

(20) Wedershoven, H.; Deuss, K.; Fantin, C.; Zeegers, J.; Darhuber, A. Active control of evaporative solution deposition by means of modulated gas phase convection. *International Journal of Heat and Mass Transfer* **2018**, *117*, 303–312.

(21) Rauch, J.; Köhler, W. Diffusion and thermal diffusion of semidilute to concentrated solutions of polystyrene in toluene in the vicinity of the glass transition. *Physical review letters* **2002**, *88*, 185901.

(22) Rubinstein, M.; Colby, R. H., et al. *Polymer physics*; Oxford university press New York, 2003; Vol. 23.

(23) Ober, R.; Paz, L.; Taupin, C.; Pincus, P.; Boileau, S. Study of the surface tension of polymer solutions: theory and experiments. Good solvent conditions. *Macromolecules* **1983**, *16*, 50–55.

(24) Toussaint, G.; Bodiguel, H.; Doumenc, F.; Guerrier, B.; Allain, C. Experimental characterization of buoyancy-and surface tension-driven convection during the drying of a polymer solution. *International Journal of Heat and Mass Transfer* **2008**, *51*, 4228–4237.

(25) Besley, L.; Bottomley, G. Vapour pressure of toluence from 273.15 to 298.15 K. *The Journal of Chemical Thermodynamics* **1974**, *6*, 577–580.

(26) Erbil, H. Y.; Avci, Y. Simultaneous determination of toluene diffusion coefficient in air from thin tube evaporation and sessile drop evaporation on a solid surface. *Langmuir* **2002**, *18*, 5113–5119.

(27) Finch, C. A. *Polymer handbook: Third edition Edited by J. Brandrup and E. H. Immergut, Wiley-Interscience, Chichester, 1989. pp. ix + parts I to VIII, price £115·00/$;175·00. ISBN 0–471–81244–7*; 1990; Vol. 23; pp 277–277, _eprint: https://onlinelibrary.wiley.com/doi/pdf/10.1002/pi.4980230318.

(28) Guerrier, B.; Bouchard, C.; Allain, C.; Bénard, C. Drying kinetics of polymer films. *AIChE Journal* **1998**, *44*, 791–798.

(29) Salez, T.; McGraw, J. D.; Bäumchen, O.; Dalnoki-Veress, K.; Raphaël, E. Capillary-driven flow induced by a stepped perturbation atop a viscous film. *Physics of Fluids* **2012**, *24*, 102111.

(30) Harris, D. J.; Lewis, J. A. Marangoni effects on evaporative lithographic patterning of colloidal films. *Langmuir* **2008**, *24*, 3681–3685.